

# Accepted Manuscript

Deconvolution-based stabilization of the incompressible Navier-Stokes equations

Alex Viguerie, Alessandro Veneziani

PII: S0021-9991(18)30768-X  
DOI: <https://doi.org/10.1016/j.jcp.2018.11.024>  
Reference: YJCPH 8377

To appear in: *Journal of Computational Physics*

Received date: 24 May 2018  
Revised date: 4 October 2018  
Accepted date: 14 November 2018

Please cite this article in press as: A. Viguerie, A. Veneziani, Deconvolution-based stabilization of the incompressible Navier-Stokes equations, *J. Comput. Phys.* (2018), <https://doi.org/10.1016/j.jcp.2018.11.024>

This is a PDF file of an unedited manuscript that has been accepted for publication. As a service to our customers we are providing this early version of the manuscript. The manuscript will undergo copyediting, typesetting, and review of the resulting proof before it is published in its final form. Please note that during the production process errors may be discovered which could affect the content, and all legal disclaimers that apply to the journal pertain.

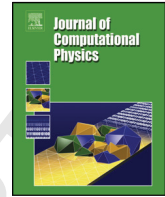


## Highlights

- New stabilization of the incompressible Navier-Stokes equations;
- Effective for cases in where standard techniques may fail;
- Works through the use of deconvolution filtering;
- Consistent and strongly consistent formulations are presented and analyzed;
- Range of two and three-dimensional test cases demonstrate effectiveness.



## Journal of Computational Physics

journal homepage: [www.elsevier.com/locate/jcp](http://www.elsevier.com/locate/jcp)Deconvolution-based stabilization of the incompressible Navier-Stokes equations<sup>\*</sup>Alex Viguerie<sup>a,\*</sup>, Alessandro Veneziani<sup>b</sup><sup>a</sup>University of Pavia, Department of Civil Engineering and Architecture, via Ferrata 3, Pavia 27100, Italy<sup>b</sup>Emory University, Department of Mathematics and Computer Science, 400 Dowman Dr NE, Atlanta 30322, Georgia USA

## ARTICLE INFO

## Article history:

## ABSTRACT

The numerical simulation of the incompressible Navier-Stokes equations may suffer from instabilities due to the energy cascades activating small-scale dynamics even when high-frequency components are not in the initial conditions. The energy cascade is generally triggered by the non-linear convective term. However, the process can be triggered by particular geometries, such that the instabilities occur even with relatively low Reynolds numbers. While instabilities for high convective fields are well known and investigated (for instance, in the framework of the *Variational Multiresolution formulation* designed by T.J. Hughes and his collaborators), numerical stabilization of low-convection instabilities is less investigated. In this paper, we present a novel method where the backbone of classical stabilizations is merged with a localization of the potentially unstable regions by means of a deconvolution-filter indicator inspired by the Large Eddie

Simulation (LES) turbulence modeling advocated by W. Layton and his collaborators. We introduce the method for steady incompressible Navier-Stokes problems, we motivate the design of the method in two different variants, the Streamline-diffusion one and the strongly consistent one. We provide some analysis of the approach and numerical results proving the improved performances in comparison with classical schemes.

© 2018 Elsevier Inc. All rights reserved.

## 1. Introduction

The incompressible Navier-Stokes problem is critical in many scientific and engineering applications, for both steady and unsteady regimes. The demand of efficient, stable, and accurate numerical solvers is consistent as more and more complex applications are nowadays faced with scientific computing tools. In fact, many challenges are open by old and new applications and the research in this field is constantly active. Among the most common difficulties are the instabilities generating spurious numerical oscillations arising from the presence of significant dynamics at small scales, unresolved by the space discretization. In the case of the steady problem, the presence of these numerical oscillations can disrupt the steady solution. In the numerical approximation, this may delay or even prevent the convergence of the nonlinear iterative solver. Sometimes, the problem is circumvented by simulating the steady problem as the limit of an unsteady simulation, however this may require a very large number of pseudo-time steps, or to use a prohibitively fine mesh.

Small-scale dynamics are often triggered by high convective fields. In this case, a number of stabilization techniques exist, in particular Streamline Diffusion, GLS and SUPG-type methods (see e.g. [8, 13, 10, 12, 23, 22, 24] for details). The classical Streamline Diffusion (or Streamline Upwind) method

<sup>☆</sup>The support of the US National Science Foundation Project: DMS-1620406 is gratefully acknowledged.

<sup>\*</sup>Corresponding author: Tel.: +1-404-727-7925; fax: +1-404-727-5611;

*e-mail:* alexander.viguerie@unipv.it (Alex Viguerie), avenez2@emory.edu (Alessandro Veneziani)

is a multidimensional generalization of the well known Upwind scheme, where a numerical viscosity - vanishing generally with the space-discretization step - is added along the direction of the convective field. GLS and SUPG belong to the family of *strongly consistent methods*, where the additional viscosity is the result of a more sophisticated procedure that guarantees the consistency with the exact solution also for the discrete problem. The additional stabilization term is generally weighted by the convective term, so these techniques are very effective in high-convection regions. Strongly consistent schemes can be regarded as an approximation of a general variational multiscale residual-based formulation of the fluid problem used in modeling the turbulence within the framework of LES models [2].

Small scale dynamics can also be triggered by other phenomena besides high convective fields. Certain geometrical features can also induce this behavior, for example recirculation in regions induced by bends, obstructions, or rough boundaries. For example, in hemodynamics, stenoses caused by atherosclerotic plaques may cause physical recirculations. We may also observe small-scale dynamics due to roughness in boundaries caused by the reconstruction of noisy data and artifacts, in which case the disturbed flow is non-physical. In both these cases, even for relatively low convective fields, we may experience instabilities for which traditional methods are not always the optimal approach. Consider for instance the 2D example of flow in a pipe with a sharp 90-degree curve. Fig. 1 displays the velocity streamlines, colored according to the velocity (inflow bottom-left, outflow top-right). The Reynolds number in this example is not exceedingly large (667), and the solution still falls within the steady regime. Nonetheless, the presence of the recirculation region along the inner wall past the curve causes stability issues, making the simulation of this test case quite challenging, requiring both a very fine mesh (at least in the region of recirculation) and a large number of iterations to converge to a steady solution. In this case, the regions causing the instability are exactly the recirculation areas, which are not a high-convective region. Therefore, stabilizing the high-convective regions as is done with SUPG or Streamline Diffusion is not necessarily the most effective strategy. In this work, we present a modified version of the aforementioned stabilization techniques, where the additional numerical viscosity is not designed on the strength and the direction of the convective field. We take inspiration from techniques developed for *LES* approaches to turbulence

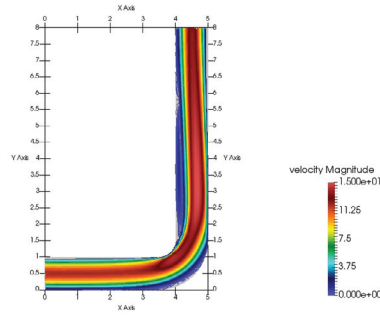


Fig. 1: Example, illustrating instabilities arising from recirculation.

modeling in order to present a different choice of the stabilization path. More specifically, the definition of the numerical viscosity is based on the deconvolution filter used for the indicator function in the LES modeling investigated in [17, 3]. This indicator function can be effective in detecting unresolved small-scale dynamics that need stabilization, even when they are not induced by high convective fields. While our stabilization method is inspired by approaches used in turbulence modeling, we note that the methods discussed here should not be regarded as turbulence models.

LES-inspired approaches for stabilizing steady incompressible flow problems by only applying stabilization to select scales have been investigated in [15, 19, 9, 16]. These methods were shown to be effective for dealing with regions of sharp flow transition, which may induce instabilities similar to those discussed here. However, these methods are still constructed by using the convective field (like SUPG and Streamline Diffusion), and therefore distinct from the approaches shown in this work.

We will begin by reviewing the construction and basic properties of standard stabilization methods. We will then introduce and analyze our LES-inspired approach, first in a consistent framework analogous to the Streamline-Diffusion method, and then in a strongly consistent formulation. We will then demonstrate the efficacy of our approach in comparison with traditional stabilizations over a series of two and three dimensional test problems. In accordance with the rest of this work, our focus here is on the Steady Navier-Stokes problem, but we also note that our findings in this section apply also to the unsteady problem.

## 2. Background: The numerical problem

Let  $\Omega \in \mathbb{R}^d$  be a suitable domain, where  $d = 2, 3$ . The steady incompressible Navier-Stokes boundary problem (for a Newtonian fluid) reads

$$\begin{aligned} -\nu \nabla \cdot (\nabla \mathbf{u} + \nabla \mathbf{u}^T) + (\mathbf{u} \cdot \nabla) \mathbf{u} + \nabla p &= \mathbf{f} \quad \text{in } \Omega \\ \nabla \cdot \mathbf{u} &= 0 \quad \text{in } \Omega \\ \mathcal{B} \mathbf{u} &= \mathbf{g} \quad \text{on } \partial\Omega, \end{aligned} \tag{2.1}$$

where  $\nu$  is the kinematic viscosity,  $\mathbf{u}$  is a  $d$ -vector representing the unknown velocity and the scalar function  $p$  is the pressure, both generally function of space. Here,  $\mathbf{f}$  is a vector-valued function representing a generic forcing term,  $\mathcal{B}$  is an appropriate trace operator defining the different types of boundary conditions of interest. In particular, we consider standard options, namely

$$\text{Dirichlet : } \mathbf{u}(\Gamma_D) = \mathbf{g}_D, \quad \text{Neumann : } (p\mathbf{n} - \nu \nabla (\mathbf{u} + \mathbf{u}^T) \cdot \mathbf{n})(\Gamma_N) = \mathbf{g}_N$$

where  $\partial\Omega = \Gamma_D \cup \Gamma_N$ ,  $\Gamma_D \cap \Gamma_N = \emptyset$ ,  $\mathbf{n}$  is the unit normal vector to the boundary and  $\mathbf{g}_D$  and  $\mathbf{g}_N$  are given. In the following, we will assume for simplicity data  $\mathbf{g} = 0$  on both Dirichlet and Neumann boundaries.

The theory of this problem is addressed e.g. in [11], Sect. IV.2, [14]. The weak formulation is promptly obtained by standard arguments. Let  $V$  be the Sobolev space  $(H_{\Gamma_D}^1)^d(\Omega)$  and  $Q = L^2(\Omega)$  (in the case  $\Gamma_N = \emptyset$ ,  $Q$  is the space  $L_0^2(\Omega)$  of the null-average  $L^2$  functions). Let us define

$$a(\cdot, \cdot) : V \times V \rightarrow \mathbb{R}, \text{ s.t. } a(\mathbf{w}, \mathbf{v}) = \nu \int_{\Omega} (\nabla \mathbf{w} + \nabla \mathbf{w}^T) : \nabla \mathbf{v}, \tag{2.2}$$

$$b(\cdot, \cdot) : V \times Q \rightarrow \mathbb{R}, \text{ s.t. } b(\mathbf{w}, q) = - \int_{\Omega} \nabla \cdot \mathbf{w} q, \tag{2.3}$$

$$c(\cdot, \cdot, \cdot) : V \times V \times V \rightarrow \mathbb{R}, \text{ s.t. } c(\mathbf{w}, \mathbf{v}, \mathbf{z}) = \int_{\Omega} (\mathbf{w} \cdot \nabla) \mathbf{v} \cdot \mathbf{z}, \tag{2.4}$$

and let  $(\cdot, \cdot)$  is the usual scalar product in  $L^2$ . Then the weak formulation of the steady problem reads:

find  $\mathbf{u} \in V$  and  $p \in Q$  s.t. for any  $\mathbf{v} \in V, q \in Q$

$$a(\mathbf{u}, \mathbf{v}) + c(\mathbf{u}, \mathbf{u}, \mathbf{v}) + b(\mathbf{v}, p) + b(\mathbf{u}, q) - (\mathbf{f}, \mathbf{v}) = 0 \quad (2.5)$$

. In particular, we recall that the bilinear form  $a(\cdot, \cdot)$  is continuous and coercive in  $V \times V$  if  $\Gamma_D \neq \emptyset$ , the trilinear form  $|c(\mathbf{w}, \mathbf{v}, \mathbf{u})|$  is continuous and, in the case of purely Dirichlet problem with divergence-free vectors, it is skew-symmetric ( $c(\mathbf{w}, \mathbf{v}, \mathbf{u}) = -c(\mathbf{w}, \mathbf{u}, \mathbf{v}) \forall \mathbf{v}, \mathbf{u} \in H_0^1(\Omega)$ .)

For the numerical solution of the problem we need to both discretize the differential operators and linearize the nonlinear quadratic convective term. In particular, we refer to the Finite Element Method (FEM), however any spatial discretization technique can be used in what follows. From now on, we denote by  $\mathbf{u}_h$  and  $p_h$  the discrete velocity and pressure belonging to finite dimensional space pair  $V_h \times Q_h$ , assumed to satisfy the so called the LBB condition [23, 11] to guarantee the well-posedness of the problem. To linearize the convective term for the steady problem, one may resort to a specific iterative method. Common methods include Picard-type and Newton-type methods, see e.g. [23] for more details. For simplicity, we refer to a Picard-type method for the remainder of this work and note that all methods discussed hold for Newton-type methods without any loss of generality.

### 3. Numerical stabilization

As the dynamics of fluids involve the interaction between large and small scales, the mesh for numerical discretization should be fine enough to resolve all scales of motion. The consequent computational cost can be prohibitively high. As an alternative to using a fine mesh, one may also employ numerical methods (“stabilizations”) to obtain reasonable solutions on coarse meshes. Techniques to stabilize (2.5) generally involve the addition of a new term to the velocity equation on each element  $K$ .

To pursue convergence, these terms must be *consistent* with the original problem; that is, the original problem is the limit of the discrete stabilized problem as  $h \rightarrow 0$  where  $h$  is the representative measure of the mesh size. There are several well-known methods that follow this general procedure, and we will focus broadly on two classes of these methods: *Streamline-diffusion methods* and *strongly consistent methods*.



The former are generally easier to implement, while the latter have the advantage of strong consistency with the original problem, leading to better convergence rates in general [8].

### 3.1. Classical Streamline-Diffusion Methods

For the purposes of generality, we will consider these methods as applied to an Oseen problem for a given vector field  $\mathbf{b}$ . This class of methods are derived from approaches originally developed for advection-diffusion-reaction problems and involve the introduction of an additional term to the momentum equation of the form  $-W_k h_K [(\mathbf{b}_h \cdot \nabla \mathbf{u}_h) \mathbf{b}_h]$ . This term adds additional viscosity to the problem along  $\mathbf{b}$ . Here  $W_k$  is a user-defined scalar function and  $h_K$  is the function representing the size of the  $K$ th mesh element. A popular example is

$$W_k \equiv \delta_K / \|\mathbf{b}\|_K, \quad (3.1)$$

where  $\delta_K$  is in turn a user-defined scalar function (often but not necessarily constant) and  $\|\mathbf{b}\|_K$  is the norm of  $\mathbf{b}$  on the current element  $K$ . Another possible choice, recommended in [27] is:

$$W_k \equiv \frac{\delta_K}{\|\mathbf{b}\|_{L^2(\Omega)}} \frac{2h_K \|\mathbf{b}\|_{L^2(K)}}{1 + h_K \|\mathbf{b}\|_{L^2(K)}} \leq \frac{2\delta_K}{\|\mathbf{b}\|_{L^2(\Omega)}} \quad (3.2)$$

Ideally, this additional diffusivity helps one gain by adding numerical viscosity along the convective field, avoiding oscillations by minimizing crosswind numerical diffusion [12, 23, 27]. In the weak form, for a given  $W_k$  and mesh size  $h_K$  it adds the form  $\tau(\cdot, \cdot, \cdot; W_k, h_K) : V_h \times V_h \times V_h \rightarrow \mathbb{R}$ , s.t. [27, 23]

$$\tau(\mathbf{b}_h, \mathbf{v}_h, \mathbf{z}_h; W_k, h_K) \equiv \sum_{K \in \mathcal{T}} W_k h_K \int_K ((\mathbf{b}_h \cdot \nabla) \mathbf{v}_h) \cdot ((\mathbf{b}_h \cdot \nabla) \mathbf{z}_h) \quad (3.3)$$

Note that for a given reticulation  $\mathcal{T}$  of a domain  $\Omega$ , for a given  $\mathbf{b}_h$ ,  $W_k > 0$  and  $h_K$ , we have

$$\tau(\mathbf{b}_h, \mathbf{v}_h, \mathbf{v}_h; W_k, h_K) = \sum_{K \in \mathcal{T}} W_k h_K \int_K \|(\mathbf{b}_h \cdot \nabla) \mathbf{v}_h\|_{L^2}^2 \geq 0, \quad |\tau(\mathbf{b}_h, \mathbf{v}_h, \mathbf{u}_h; W_k, h_K)| \leq C \|\mathbf{b}_h\|_V^2 \|\mathbf{v}_h\|_V \|\mathbf{z}_h\|_V. \quad (3.4)$$

The weak formulation of the stabilized problem reads: given  $\mathbf{b}_h$  regular enough, find  $\mathbf{u}_h \in V$  and  $p_h \in Q$  s.t. for any  $\mathbf{v}_h \in V_h, q_h \in Q_h$ :

$$\begin{aligned} a(\mathbf{u}_h, \mathbf{v}_h) + c(\mathbf{b}_h, \mathbf{u}_h, \mathbf{v}_h) + b(\mathbf{v}_h, p_h) + \\ \tau(\mathbf{b}_h, \mathbf{u}_h, \mathbf{v}_h; W_K, h_K) + b(\mathbf{u}_h, q_h) - (\mathbf{f}, \mathbf{v}_h) = 0 \end{aligned} \quad (3.5)$$

The well-posedness of this problem follows from the well-posedness of (2.5) under standard assumptions [11, 23, 8, 22, 12, 27] and (3.4). Referring to (3.3), we note for each element  $K$ , the form  $\tau$  depends on the element diameter  $h_K$ . As the mesh is refined  $h_{MAX} \equiv \max_K(h_K) \rightarrow 0$ , it follows that  $\tau \rightarrow 0$  everywhere in  $\mathcal{T}$ . This establishes the consistency of these stabilization methods, as the numerical problem converges to the original one when the mesh size vanishes.

One obtains a stabilized Picard-type iteration for the Navier-Stokes problem in the obvious way by setting  $\mathbf{b}_h = \mathbf{u}_h^k$  in (3.5) at an iteration  $k + 1$ . This method works by adding artificial viscosity only in the direction of the solution streamlines. It can be regarded as a generalization of the *upwinding methods* common in one-dimensional problems. For this reason it is also referred to as the *streamlined upwinding method* in the literature [8, 12].

Classical Streamline Diffusion is often over-diffusive; while this can reduce the instabilities so to accelerate the convergence to a steady solution, it adversely affects the accuracy. Strongly consistent methods alleviate this problem [8, 12].

### 3.2. Strongly Consistent Methods

*Strongly consistent methods* [13, 10, 22] work by the addition of the strong element-wise formulation of a residual term of  $\mathcal{L}_h(\mathbf{u}_h, p_h; \mathbf{b}_h, \mathbf{f}, \mathbf{v}_h, q_h)$  to the problem (2.5), i.e. a stabilizing term such that

$$\mathcal{L}_h(\mathbf{u}, p; \mathbf{b}_h, \mathbf{f}, \mathbf{v}_h, q_h) = 0 \quad \forall (\mathbf{v}_h, q_h) \in V_h \times Q_h \quad (3.6)$$

where  $(\mathbf{u}, p)$  is the exact solution to (2.5). Hence, the true solution satisfies the stabilized problem exactly and not just asymptotically, as in the previous case. Consequently, these methods are generally more accurate than the classical streamline-diffusion type methods [23]. In fact, convergence rate - in an appro-

appropriate norm - depends on the degree of the finite elements used, which is generally not true for classical Streamline Diffusion. This comes at a cost, however, and these methods are often more difficult to formulate and implement, and in our experience may negatively affect the conditioning of the associated linear systems. Two common methods of this type are the *Streamlined Upwind Galerkin Method* (SUPG) and the *Galerkin Least-Squares Method* (GLS). For the sake of brevity, we limit here only to SUPG.

For the steady Navier-Stokes problem, we let  $\mathcal{L}_h$  be defined as (setting  $\mathbf{b}_h = \mathbf{u}_h$ ):

$$\begin{aligned} \mathcal{L}_h(\mathbf{u}_h, p_h; \mathbf{u}_h, \mathbf{f}, \mathbf{v}_h, q_h) = \\ \sum_{K \in \mathcal{T}_h} \delta_K (-\nu \Delta \mathbf{u}_h + (\mathbf{u}_h \cdot \nabla) \mathbf{u}_h + \nabla p_h - \mathbf{f}, (\mathbf{u}_h \cdot \nabla) \mathbf{v}_h + \nabla q_h)_{L^2(K)}. \end{aligned} \quad (3.7)$$

Here,  $\delta_K$  is an element-wise constant parameter defined by the user and is generally dependent on the mesh size. The well-posedness of these and other similar formulations is shown in [24]. In addition to their general convective stabilizing properties, methods of this type enjoy the additional property of stabilizing non-LBB inf-sup compatible element pairs for velocity and pressure (for example,  $\mathbb{P}^1/\mathbb{P}^1$ ) [24].

#### 4. LES-inspired stabilization

*Generalized Leray models* [20] for Large Eddy simulation explored in [17, 3] work by the construction of a *filtered field*  $\bar{\mathbf{u}}$  which identifies regions where the solution requires stabilization. In the context of turbulence modeling, the idea of this filtering step is the identification of relevant small scales, unresolved by the space discretization. In this way, by construction,  $\bar{\mathbf{u}}$  is small in regions where  $\mathbf{u}$  is “smooth” and large where  $\mathbf{u}$  is “not smooth”, indicating where the fluid velocity can be simulated directly and where small scales should be modeled. We borrow from this idea to develop our stabilization technique. We focus particularly on the steady problem here, even though the idea of ‘large eddy simulation’ is inherently unsteady. The application of such techniques to steady problems represents, in fact, a novel approach.

Given an appropriate filter function that will be specified later  $F(\cdot)$  and an available velocity field  $\mathbf{u}^k$  we can apply the following algorithm at an iteration  $k + 1$  to promptly obtain a modified stabilization scheme:

1. Compute  $\bar{u}^{k+\frac{1}{2}} = F u^k$ ;
2. Solve (3.5) with a stabilization term guided by the filtered field  $\bar{u}^{k+\frac{1}{2}}$ ;
3. Check Convergence of nonlinear iteration: end if criterion met; else update and loop.

A major difference between the approach discussed in this work and the existing methods for LES is that we use the filtered field to construct an alternative stabilization, not to activate turbulence modeling. While in the existing literature, it is used in conjunction with a differential filter to obtain a regularized convective field for the current time step or as part of an evolution/relaxation scheme [3] we use the indicator function directly in a streamline diffusion-style manner as in (3.5).

To motivate our deconvolution-based approach, we return to the same two-dimensional example shown in the introduction. Observe the plot of  $\bar{u}$  for the same problem, obtained by applying a non-linear deconvolution-based filter to  $u$  function similar to those described in [5, 3], as we detail hereafter - see Fig. 2, right panel.

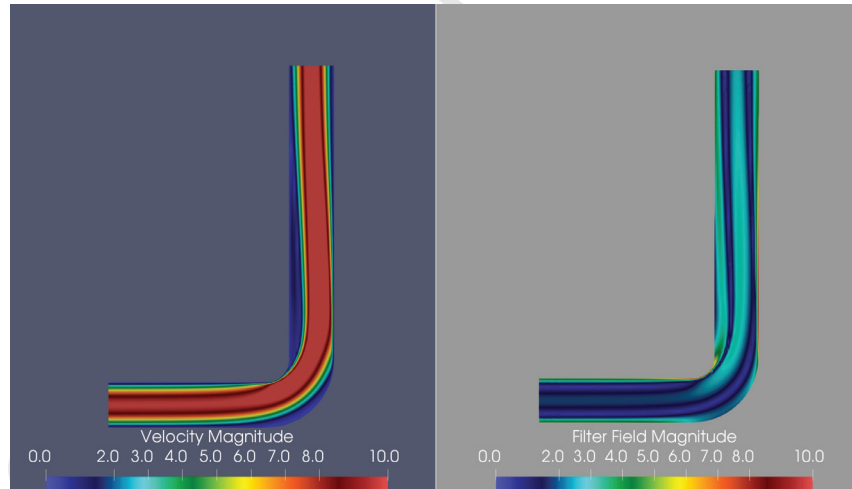


Fig. 2: A simplified example of small-scale dynamics induced by the geometry of a domain with a relatively low Reynolds number. Left: velocity field  $u$  in a bending pipe. Right: filtered field  $\bar{u} = F u$  with  $F$  specified in the text.

The figure illustrates why stabilizing along the vector field  $\bar{u}$  is preferable to the traditional streamline-diffusion scheme; the recirculation region is no longer neglected. Thus, when we add numerical viscosity along  $\bar{u}$ , we are now adding it to the small-scale and then potentially unstable area, which does not happen when using traditional streamline-based techniques.

Many filters have been investigated in the literature. These filters may be physics-based, such as those discussed in [17, 5] or may arise from mathematical arguments, as in [4, 3]. In this work we focus our attention on *deconvolution-based nonlinear filters*, which belong to this latter group [18].

Let  $V$  be a Hilbert space and  $L : V \rightarrow V$  be a linear, invertible, self-adjoint, compact operator. By the spectral theorem (see e.g. [25]), we have:

$$Lu = \sum_{i=0}^{\infty} \lambda_i \langle u, e_i \rangle e_i, \quad L^{-1}u = \sum_{i=0}^{\infty} \frac{1}{\lambda_i} \langle u, e_i \rangle e_i \quad (4.1)$$

where  $\{e_i\}_{i=0}^{\infty}$  are eigenfunctions of  $F$  and form an orthonormal basis for  $V$ . Since  $F$  is compact, it follows that  $F^{-1}$  is unbounded. Let  $D$  be a bounded, finite-dimensional truncation of  $L^{-1}$ . In regions where  $u$  is smooth, we expect that  $\langle u, e_i \rangle$  is only significant for small values of  $i$ . We may then define the indicator function based on the definition  $Fu \equiv u - D(Lu)$ . We expect  $Fu$  to be ‘small’ in the regions where  $u$  is smooth and ‘large’ where  $u$  is not smooth (ie, where  $u$  requires regularization).

A popular choice for  $D$  is the *Van Cittert deconvolution operator*, given by:

$$D_N = \sum_{n=0}^N (I - L)^n \quad (4.2)$$

$N$  is typically small, and in this work we will use  $N = 0$ , so that  $F_{D_0} = u - L(u)$ . We define  $L$  as the linear *Helmholtz filter operator*  $L_H$ :

$$L_H = \left( I - \mu^2 \Delta \right)^{-1} \quad (4.3)$$

where  $\mu > 0$  is the *filtering radius* and  $\Delta$  is the Laplacian:  $\Delta = \sum_{j=1}^d \frac{\partial^2}{\partial x_j^2}$  where  $d = 2, 3$  is the number of spatial dimensions.

*Prescription of the boundary conditions for the nonlinear filter  $L_H$ .* The filtering problem requires the prescription of boundary conditions to be well-posed. While setting  $L(u) = u$  everywhere on the boundary is common for LES filtering, for this problem this choice does not yield optimal results. In fact, the auxiliary field obtained by the filtering is intended to identify regions that may be in proximity of the boundary.

As the essential no-slip condition on  $\mathbf{u}$  limits the variability of  $L(\mathbf{u})$  near the walls, this is not ideal for our purposes. The recirculation regions generally occur near walls and therefore we want to allow  $L(\mathbf{u})$  to be possibly large in these regions. We opted for homogeneous Neumann conditions here. To take advantage from the Poincaré inequality, which is helpful for the analysis, we then let  $L(\mathbf{u}) = \mathbf{u}$  on the outflows. This choice has no practical counterindications.

We then have a sort of rule-of-thumb for the selection of the boundary conditions for the filter operator, in which we set natural conditions where the physical field is subject to Dirichlet conditions and vice versa. This is a purely numerical choice, and we do not ascribe to it any physical meaning. We stress that  $\bar{\mathbf{u}}$  has significance only as an auxiliary numerical tool. As the name “filtered velocity” can be misleading and may imply a physical interpretation, we will instead use the term “filtered field”.

**Remark 4.1.** Some properties of the filter operator are immediately deduced once we establish the link between the filtering operator  $F$  and the Yosida regularization of the Laplace operator  $-\Delta$  associated with the boundary conditions specified above. Following [6] and Chap. 7 of [7],  $L_H$  is the so-called resolvent of  $-\Delta$  and  $\mu^{-2}F$  its Yosida regularization. Notice that the domain of the resolvent is  $L^2(\Omega)$  and that the norm of the resolvent as linear and continuous operator on  $L^2$  is  $\leq 1$ .

From this general theory, in particular it is possible to prove that for any  $\mu \neq 0$ :

- (a)  $\mu^{-2}F = -L_H(\Delta)$  for any field in  $H^1(\Omega)$ ;
- (b)  $\|\mu^{-2}F\mathbf{v}\|_{L^2} \leq \|-\Delta\mathbf{v}\|_{L^2}$  for any velocity field  $\mathbf{v}$  in  $H^1$ ;
- (c)  $(F\mathbf{v}, \mathbf{v}) \geq 0$  for any field  $\mathbf{v}$  in  $L^2$ ;
- (d)  $\|F\mathbf{v}\|_{L^2} \leq \|\mathbf{v}\|_{L^2}$  for any field  $\mathbf{v}$  in  $L^2$ .

These properties emphasize that the filtered field pursues a non-negative (dissipative) action (property (c)), with a regularizing action milder than the one of the Laplace operator ((b)).

*On the divergence of the filtered field.* In absence of boundaries (i.e. periodic boundary conditions) and with the constant-coefficient operator  $L_H$ , we can verify that for a divergence-free vector field  $\mathbf{u}$ , the filtered field  $\bar{\mathbf{u}} = F\mathbf{u}$  is also divergence free. In fact, from property (a) listed above and the commutativity of the Laplace and divergence operators.

$$L_H^{-1}F\mathbf{u} = -\mu^2(\Delta)\mathbf{u}$$

so that if  $\nabla \cdot \mathbf{u} = 0$ ,  $\nabla \cdot (L_H^{-1}F\mathbf{u}) = 0$ . Recalling that  $L_H^{-1} = I - \mu^2\Delta$  is a constant-coefficient operator, then  $\nabla \cdot (L_H^{-1}F\mathbf{u}) = L_H^{-1}(\nabla \cdot F\mathbf{u}) = 0$  from which for periodic boundary conditions we conclude that  $F\mathbf{u}$  is divergence free.

In the general and realistic case of a boundary value problem, we speculate (and verified) that the divergence of the filtered velocity is small. Also, at the discrete level, the finite element pair of spaces  $V_h, Q_h$  does not guarantee that a weakly divergence-free field is also strongly divergence-free. In fact, we notice that  $\forall q \in Q_h$

$$\int_{\Omega} \nabla \cdot F \mathbf{u}_h q_h = \int_{\Omega} \nabla \cdot \mathbf{u}_h q_h - \mu^2 \int_{\Omega} \nabla \cdot L_H \mathbf{u}_h q_h = -\mu^2 \int_{\Omega} \nabla \cdot L_H \mathbf{u}_h q_h.$$

This implies that the weak divergence scales with  $\mu^2$ .

We also prove the following Theorem.

**Theorem 4.2.** For a given velocity field  $\mathbf{u}$  in  $H^2(\Omega) \cap H_0^1(\Omega)$ ,  $\|F\mathbf{u}\|_V \leq \|\mathbf{u}\|_V$ .

**Proof.** From the definition of  $F$ ,

$$F\mathbf{u} = \mathbf{u} - (I - \mu^2 \Delta)^{-1} \mathbf{u} \quad (4.4)$$

Let  $\mathbf{w}$  in  $H^2(\Omega)$  with  $\mathbf{w} \equiv (I - \mu^2 \Delta)^{-1} \mathbf{u}$ , then

$$(I - \mu^2 \Delta) \mathbf{w} = \mathbf{u}, \quad \Delta \mathbf{w} = \frac{1}{\mu^2} (\mathbf{w} - \mathbf{u}) = -\frac{1}{\mu^2} F\mathbf{u} \quad (4.5)$$

From (4.4), and (4.5) we have have that  $F\mathbf{u}$  solves the following variational problem: Find  $F\mathbf{u}$  in  $H^2(\Omega)$  such that for all  $\mathbf{v}$  in  $H^2(\Omega)$ ,

$$-\int_{\Omega} F\mathbf{u} \cdot \mathbf{v} = -\int_{\Omega} \mathbf{u} \cdot \mathbf{v} + \int_{\Omega} \mathbf{w} \cdot \mathbf{v} \quad (4.6)$$

Let  $\mathbf{v} = \Delta F\mathbf{u}$ . Integration by parts with the boundary conditions specified above gives:

$$\begin{aligned} \|\nabla F\mathbf{u}\|_{L^2}^2 &= \int_{\Omega} \nabla \mathbf{u} : \nabla F\mathbf{u} - \int_{\Omega} \nabla \mathbf{w} : \nabla F\mathbf{u} = \int_{\Omega} \nabla \mathbf{u} : \nabla F\mathbf{u} + \int_{\Omega} \Delta \mathbf{w} \cdot F\mathbf{u} \\ &= \int_{\Omega} \nabla \mathbf{u} : \nabla F\mathbf{u} - \frac{1}{\mu^2} \|F\mathbf{u}\|_{L^2}^2 \end{aligned} \quad (4.7)$$

Discarding the strictly positive second term on the right-hand side above and applying Cauchy-Schwarz

then gives  $\|\nabla F u\|_{L^2} \leq \|\nabla u\|_{L^2}$ , which by equivalence of the norms  $\|\nabla v\|_{L^2}$  and  $\|v\|_V$ , was to be shown.

#### 4.1. Filtered-Streamline Diffusion

The filtered field  $\bar{u}$  is used in our modified classical streamline diffusion scheme instead of the velocity field  $u$ . In an iterative Picard scheme, this leads to the following algorithm, a particularization of the one introduced at the beginning of the present section. At each iteration we solve the stabilized problem:

Find  $u_h^{k+1}$  in  $V_h$ ,  $p_h^{k+1}$  in  $Q_h$  such that for all  $v_h$  in  $V_h$ ,  $q_h$  in  $Q_h$ :

$$\begin{aligned} a(u_h^{k+1}, v_h) + c(u_h^k, u_h^{k+1}, v_h) + b(v_h, p_h^{k+1}) \\ + b(u_h^{k+1}, q_h) + \tau(\bar{u}_h^{k+\frac{1}{2}}, u_h^{k+1}, v_h; W_K, h_K) - (f, v_h) = 0 \end{aligned} \quad (4.8)$$

Note that, unlike in (3.5), the convective field  $u_h^k$  in the trilinear form  $c$  is not the same as the convective field  $\bar{u}_h^{k+\frac{1}{2}}$  in the stabilization term  $\tau$ . However, the properties (3.4) still hold, coercivity trivially and continuity from property (d) in Remark (4.1). The iteration (4.8) is therefore still well posed for given  $u_h^k$  and  $\bar{u}_h^{k+\frac{1}{2}}$ . Because of this distinction, it is somewhat ambiguous whether we should define  $W_K$  based on the norm of the physical velocity  $\|u_h\|$  or the filter field  $\|\bar{u}_h\|$ ; we found both approaches effective in our numerical experiments but somewhat better performance when using the physical velocity.

This method requires the solution of the Helmholtz system at each iteration. This represents an additional cost; however we note that the Helmholtz operator does not change throughout during the iterative scheme and therefore the associated matrix need only be assembled once. A solution of this problem is therefore an arguably small fraction of the cost of full Picard iteration on the saddle-point system; in some tests we found it to be less than one percent of the computational time. Accordingly, if the stabilized method allows for convergence in fewer iterations, we do not expect the cost of the filter problem to offset these savings.

##### 4.1.1. Convergence Proof

Here we present a convergence proof for the iteration (4.8). This proof is inspired heavily by the convergence proof of the standard Picard method found in [14]. As is standard in these analyses, we assume



homogenous Dirichlet boundary conditions for the physical velocity  $\mathbf{u}_h$ . Since we will be performing operations with  $\tau$ , we will express it as a quadrilinear form in order to make these manipulations more clear. For ease of notation, we write  $\tau(\mathbf{w}_h, \mathbf{v}_h, \mathbf{y}_h, \mathbf{z}_h; W_K, h_K)$  as simply  $\tau(\mathbf{w}_h, \mathbf{v}_h, \mathbf{y}_h, \mathbf{z}_h)$ , with the dependence on the parameter  $W_K$  and mesh size  $h_K$  understood. For simplicity, we will assume that the bilinear form  $a$  is written in its *Laplacian form*:

$$a(\cdot, \cdot) : V \times V \rightarrow \mathbb{R}, \text{ s.t. } a(\mathbf{w}, \mathbf{v}) = \nu \int_{\Omega} \nabla \mathbf{u} : \nabla \mathbf{v}, \quad (4.9)$$

and note that the same result holds for the full-tensor by Korn's Inequality.

Denote as  $X_h \subset V_h$  the set of weakly-divergence free vectors:

$$X_h := \{\mathbf{v}_h \in V_h, b(\mathbf{v}_h, q_h) = 0 \forall q_h \in Q_h\}. \quad (4.10)$$

We define the *consistent Deconvolution-stabilized Navier-Stokes problem* as: find  $\mathbf{u}_h$  in  $V_h$ ,  $p_h$  in  $Q_h$  such that for all  $\mathbf{v}_h$  in  $V_h$ ,  $q_h$  in  $Q_h$ :

$$a(\mathbf{u}_h, \mathbf{v}_h) + c(\mathbf{u}_h, \mathbf{u}_h, \mathbf{v}_h) + b(\mathbf{v}_h, p_h) + b(\mathbf{u}_h, q_h) + \tau(\bar{\mathbf{u}}_h, \mathbf{u}_h, \mathbf{v}_h; W_K, h_K) - (\mathbf{f}, \mathbf{v}_h) = 0 \quad (4.11)$$

The velocity solution  $\mathbf{u}_h$  of (4.11) satisfies the bound [26, 14]:

$$\|\mathbf{u}_h\|_V \leq \frac{\|\mathbf{f}\|_{-1}}{\nu C_a}, \quad (4.12)$$

The solution to the problem (4.11) is unique assuming the following small data condition holds [26, 14] :

$$\chi \equiv \frac{\nu^2 C_a^2}{C_b \|\mathbf{f}\|_{-1}} > 1. \quad (4.13)$$

**Theorem 4.1.** *Let us assume that there exists a unique solution pair  $(\mathbf{u}_h, p_h)$  pair to (4.11), resulting from regularity assumptions and the small data hypothesis (4.13). Assume data sufficiently regular such that  $\mathbf{u}_h \in H^2(\Omega)$ . Then the sequence given by (4.8) converges to  $(\mathbf{u}_h, p_h)$  provided the initial guess  $(\mathbf{u}_h^0, p_h^0)$  is sufficiently close and*

$\delta_K$  is chosen such that:

$$\delta_K < \frac{C_b(\chi - 1)}{2h_{MAX}} \quad (4.14)$$

is satisfied, where  $h_{MAX}$  is the size of the largest element in  $\mathcal{T}$ .

**Proof.**

We proceed by induction. Denote  $\mathbf{e}^k := \mathbf{u}_h^k - \mathbf{u}_h$  and  $\bar{\mathbf{e}}^k := \bar{\mathbf{u}}_h^{k+\frac{1}{2}} - \bar{\mathbf{u}}_h$ . We assume at an iteration  $k$  for some  $\tilde{\chi} > 1$ ,

$$\|\mathbf{e}^k\|_V \leq \frac{1}{\tilde{\chi}^k} \|\mathbf{e}^0\|_V \quad (4.15)$$

and we seek to show that:

$$\|\mathbf{e}^{k+1}\|_V \leq \frac{1}{\tilde{\chi}} \|\mathbf{e}^k\|_V \leq \frac{1}{\tilde{\chi}^{k+1}} \|\mathbf{e}^0\|_V \quad (4.16)$$

Based on the fact that  $\|\bar{\mathbf{u}}_h\|_{L^2} \leq \|\mathbf{u}_h\|_{L^2}$  (see Remark 4.1), we assume additionally that for an initial guess close enough:

$$\|\bar{\mathbf{u}}_h^{k+\frac{1}{2}}\|_{L^2} \leq \|\mathbf{u}_h\|_{L^2} \quad (4.17)$$

Begin by subtracting (4.11) from (4.8) at the iteration  $k+1$  to obtain:

$$\begin{aligned} & a(\mathbf{e}^{k+1}, \mathbf{v}_h) + b(\mathbf{v}_h, p_h^{k+1} - p_h) + b(\mathbf{e}^{k+1}, q_h) + c(\mathbf{u}_h^k, \mathbf{u}_h^{k+1}, \mathbf{v}_h) - c(\mathbf{u}_h, \mathbf{u}_h, \mathbf{v}_h) \\ & + \tau(\bar{\mathbf{u}}_h^{k+\frac{1}{2}}, \mathbf{u}_h^{k+1}, \bar{\mathbf{u}}_h^{k+\frac{1}{2}}, \mathbf{v}_h) - \tau(\bar{\mathbf{u}}_h, \mathbf{u}_h, \bar{\mathbf{u}}_h, \mathbf{v}_h) = 0 \end{aligned} \quad (4.18)$$

Noting that  $\mathbf{e}^{k+1}$  is in the space  $X_h$  (4.10) implies  $b(\mathbf{e}^{k+1}, q_h) = 0$ . After some rearrangement and adding and subtracting  $c(\mathbf{u}_h^k, \mathbf{u}_h, \mathbf{v}_h)$ ,  $\tau(\bar{\mathbf{u}}_h^{k+\frac{1}{2}}, \mathbf{u}_h, \bar{\mathbf{u}}_h^{k+\frac{1}{2}}, \mathbf{v}_h)$ , and  $\tau(\bar{\mathbf{u}}_h^{k+\frac{1}{2}}, \mathbf{u}_h, \bar{\mathbf{u}}_h, \mathbf{v}_h)$ :

$$\begin{aligned} & a(\mathbf{e}^{k+1}, \mathbf{v}_h) + b(\mathbf{v}_h, p_h^{k+1} - p_h) + \tau(\bar{\mathbf{u}}_h^{k+\frac{1}{2}}, \mathbf{e}^{k+1}, \bar{\mathbf{u}}_h^{k+\frac{1}{2}}, \mathbf{v}_h) = \\ & -c(\mathbf{e}^k, \mathbf{u}_h, \mathbf{v}_h) - c(\mathbf{u}_h^k, \mathbf{e}^{k+1}, \mathbf{v}_h) - \tau(\bar{\mathbf{u}}_h^{k+\frac{1}{2}}, \mathbf{u}_h, \bar{\mathbf{e}}^k, \mathbf{v}_h) - \tau(\bar{\mathbf{e}}^k, \mathbf{u}_h, \bar{\mathbf{u}}_h, \mathbf{v}_h) \end{aligned} \quad (4.19)$$

We now let  $\mathbf{v}_h = \mathbf{e}^{k+1}$ . This gives  $b(\mathbf{e}^{k+1}, p_h^{k+1} - p_h) = 0$  by  $\mathbf{e}^{k+1} \in X_h$  and  $c(\mathbf{u}_h^k, \mathbf{e}^{k+1}, \mathbf{e}^{k+1}) = 0$  by skew-symmetry, yielding:

$$\begin{aligned} & \nu C_a \|\mathbf{e}^{k+1}\|_V^2 + W_K h_{MIN} \|(\bar{\mathbf{u}}_h^{k+\frac{1}{2}} \cdot \nabla) \mathbf{e}^{k+1}\|_{L^2}^2 \\ & \leq C_b \|\mathbf{e}^k\|_V \|\mathbf{u}_h\|_V \|\mathbf{e}^{k+1}\|_V + \sum_{K \in \mathcal{T}} W_K h_K \|(\bar{\mathbf{u}}_h^{k+\frac{1}{2}} \cdot \nabla) \mathbf{u}_h\|_{L^2(K)} \|(\bar{\mathbf{e}}^k \cdot \nabla) \mathbf{e}^{k+1}\|_{L^2(K)} \\ & \quad + \sum_{K \in \mathcal{T}} W_K h_K \|(\bar{\mathbf{e}}^k \cdot \nabla) \mathbf{u}_h\|_{L^2(K)} \|(\bar{\mathbf{u}}_h \cdot \nabla) \mathbf{e}^{k+1}\|_{L^2(K)} \end{aligned} \quad (4.20)$$

Applying the Cauchy-Schwarz inequality on the summation terms above gives:

$$\begin{aligned} & \nu C_a \|\mathbf{e}^{k+1}\|_V^2 + W_K h_{MIN} \|(\bar{\mathbf{u}}_h^{k+\frac{1}{2}} \cdot \nabla) \mathbf{e}^{k+1}\|_{L^2}^2 \\ & \leq C_b \|\mathbf{e}^k\|_V \|\mathbf{u}_h\|_V \|\mathbf{e}^{k+1}\|_V + W_K h_{MAX} \|(\bar{\mathbf{u}}_h^{k+\frac{1}{2}} \cdot \nabla) \mathbf{u}_h\|_{L^2} \|(\bar{\mathbf{e}}^k \cdot \nabla) \mathbf{e}^{k+1}\|_{L^2} \\ & \quad + W_K h_{MAX} \|(\bar{\mathbf{e}}^k \cdot \nabla) \mathbf{u}_h\|_{L^2} \|(\bar{\mathbf{u}}_h \cdot \nabla) \mathbf{e}^{k+1}\|_{L^2} \\ & \leq C_b \|\mathbf{e}^k\|_V \|\mathbf{u}_h\|_V \|\mathbf{e}^{k+1}\|_V + W_K h_{MAX} \|\bar{\mathbf{u}}_h^{k+\frac{1}{2}}\|_{L^2} \|\nabla \mathbf{u}_h\|_{L^2} \|\bar{\mathbf{e}}^k\|_{L^2} \|\nabla \mathbf{e}^{k+1}\|_{L^2} \\ & \quad + W_K h_{MAX} \|\bar{\mathbf{e}}^k\|_{L^2} \|\nabla \mathbf{u}_h\|_{L^2} \|\bar{\mathbf{u}}_h\|_{L^2} \|\nabla \mathbf{e}^{k+1}\|_{L^2} \end{aligned} \quad (4.21)$$

where the last line follows from the basic inequality:  $\|(\mathbf{w} \cdot \nabla) \mathbf{v}\|_{L^2} \leq \|\mathbf{w}\|_{L^2} \|\nabla \mathbf{v}\|_{L^2}$ . Let  $W_K$  be such that:

$$W_K := \delta_K / \|\mathbf{u}_h\|_{L^2} \quad (4.22)$$

Then from (4.22), (4.17),  $\|\bar{\mathbf{u}}_h\|_{L^2} < \|\mathbf{u}_h\|_{L^2}$  and Theorem 4.2, (4.23) reduces to:

$$\begin{aligned} & \nu C_a \|\mathbf{e}^{k+1}\|_V^2 + W_K h_{MIN} \|(\bar{\mathbf{u}}_h^{k+\frac{1}{2}} \cdot \nabla) \mathbf{e}^{k+1}\|_{L^2}^2 \\ & \leq (C_b + 2\delta_K h_{MAX}) \|\mathbf{e}^k\|_V \|\mathbf{u}_h\|_V \|\mathbf{e}^{k+1}\|_V \\ & \leq (C_b + 2\delta_K h_{MAX}) \frac{\|\mathbf{f}\|_{-1}}{\nu C_a} \|\mathbf{e}^k\|_V \|\mathbf{e}^{k+1}\|_V \end{aligned} \quad (4.23)$$

where the last line follows from (4.12). Then from (4.13):

$$\|e^{k+1}\|_V + W_K h_{MIN} \frac{\|(\tilde{u}_h^{k+\frac{1}{2}} \cdot \nabla) e^{k+1}\|_{L^2}^2}{\nu C_a \|e^{k+1}\|_V} \leq \left( \frac{1}{\tilde{\chi}} + \frac{2\delta_K h_{MAX} \|f\|_{-1}}{\nu^2 C_a^2} \right) \|e^k\|_V \quad (4.24)$$

Which implies the result if:

$$\tilde{\chi} \equiv \frac{\nu^2 C_a^2}{(C_b + 2\delta_K h_{MAX}) \|f\|_{-1}} > 1 \quad (4.25)$$

This holds provided

$$\delta_K < \frac{C_b(\tilde{\chi} - 1)}{2 h_{MAX}} \quad (4.26)$$

Note the right hand side of (4.26) is guaranteed to be positive by (4.13). Verification that the base case holds for  $u_h^0 = 0$  using similar arguments as above is straightforward and omitted for the sake of brevity.

While (4.24) immediately implies (4.16), looking at its left hand side shows that it in fact establishes a stronger result that explains how this method stabilizes. By the established bounds, we may assume that for large enough  $k$ :

$$\|e^{k+1}\|_V \leq \frac{W_K h_{MIN}}{\nu C_a}, \text{ implying: } 1 \leq \frac{W_K h_{MIN}}{\nu C_a \|e^{k+1}\|_V} \quad (4.27)$$

By which one obtains:

$$\|e^{k+1}\|_V + \|(\tilde{u}_h^{k+\frac{1}{2}} \cdot \nabla) e^{k+1}\|_{L^2}^2 \leq \frac{1}{\tilde{\chi}} \|e^k\|_V \quad (4.28)$$

Note that the contraction constant  $\tilde{\chi}^{-1}$  is similar to the constant  $\chi^{-1}$  in the standard (non-stabilized) Picard iteration [14], but is now bounding two positive terms dependent on  $e^{k+1}$ : the error in the  $H^1$  norm  $\|e^{k+1}\|_V$  as well as the error along the filtered field  $\|(\tilde{u}_h^{k+\frac{1}{2}} \cdot \nabla) e^{k+1}\|_{L^2}^2$ . Based on this, we expect the stabilization term to accelerate convergence by providing stronger control on the error in the regions identified by  $\tilde{u}_h^{k+\frac{1}{2}}$ . This is confirmed by our numerical experiments.

#### 4.2. A Strongly Consistent Method

Applying this approach to strongly consistent methods is not immediate. Classical strongly consistent methods rely on the residual:

$$-v\Delta \mathbf{u} + (\mathbf{u} \cdot \nabla) \mathbf{u} + \nabla p - \mathbf{f} \quad (4.29)$$

Implicit in this definition is the reliance on the streamline vector field  $\mathbf{u}$ , which serves both as the stabilization path and to guarantee strong consistency. Putting  $\bar{\mathbf{u}} = \mathbf{u} - D(L\mathbf{u})$  in the convective term of (4.29) gives:

$$-v\Delta \mathbf{u} + (\mathbf{u} \cdot \nabla) \mathbf{u} - (D(L(\mathbf{u})) \cdot \nabla) \mathbf{u} + \nabla p - \mathbf{f} \quad (4.30)$$

which will be nonzero when evaluated at the exact solution in general. We therefore need a term to offset the contributions of  $(D(L(\mathbf{u})) \cdot \nabla) \mathbf{u}$  in order for (4.30) to be consistent with (4.29). Let  $\hat{\mathbf{u}} = D(L(\mathbf{u}))$  for the sake of notation and note that  $\hat{\mathbf{u}} = \mathbf{u} - \bar{\mathbf{u}}$ . We then take advantage of our iterative framework and at a given iteration  $k+1$  we introduce the following two bilinear forms (*FIL* stands for “filtered” and *EXP* for “explicit”):

$$\begin{aligned} \mathcal{L}_{FIL}(\mathbf{u}_h^{k+1}, p_h^{k+1}; \bar{\mathbf{u}}_h^{k+\frac{1}{2}}, \mathbf{f}, \mathbf{v}_h, q_h) = \\ \sum_{K \in \mathcal{T}_h} h_K W_K \left( -v\Delta \mathbf{u}_h^{k+1} + (\bar{\mathbf{u}}_h^{k+\frac{1}{2}} \cdot \nabla) \mathbf{u}_h^{k+1} + \nabla p_h^{k+1} - \mathbf{f}, (\bar{\mathbf{u}}_h^{k+\frac{1}{2}} \cdot \nabla) \mathbf{v}_h + \nabla q_h \right)_{L^2(K)} \\ \mathcal{L}_{EXP}(\mathbf{u}_h^k, \hat{\mathbf{u}}_h^{k+\frac{1}{2}}, \bar{\mathbf{u}}_h^{k+\frac{1}{2}}, \mathbf{v}_h, q_h) = \\ \sum_{K \in \mathcal{T}_h} h_K W_K \left( (\hat{\mathbf{u}}_h^{k+\frac{1}{2}} \cdot \nabla) \mathbf{u}_h^k, (\bar{\mathbf{u}}_h^{k+\frac{1}{2}} \cdot \nabla) \mathbf{v}_h + \nabla q_h \right)_{L^2(K)} \end{aligned} \quad (4.31)$$

The term  $\mathcal{L}_{EXP}$  is entirely explicit. For a convergent iterative scheme  $\mathbf{u}_h^{k+1} \approx \mathbf{u}_h^k$ , and  $\mathcal{L}_{EXP}$  negates the contributions of  $(\hat{\mathbf{u}}_h^{k+1} \cdot \nabla) \mathbf{u}_h^{k+1}$  without affecting the coercivity of  $\mathcal{L}_{FIL}$ . Then at each step we solve the

following problem: Find  $(\mathbf{u}_h^{k+1}, p_h^{k+1})$  in  $V_h \times Q_h$  such that

$$\begin{aligned} a(\mathbf{u}_h^{k+1}, \mathbf{v}_h) + c(\mathbf{u}_h^k, \mathbf{u}_h^{k+1}, \mathbf{v}_h) + b(\mathbf{v}_h, p_h^{k+1}) + b(\mathbf{u}_h^{k+1}, q_h) + \\ \mathcal{L}_{FIL}(\mathbf{u}_h^{k+1}, p_h^{k+1}; \bar{\mathbf{u}}_h^{k+\frac{1}{2}}, \mathbf{f}; \mathbf{v}_h, q_h) = -\mathcal{L}_{EXP}(\mathbf{u}_h^k, \hat{\mathbf{u}}_h^{k+\frac{1}{2}}, \bar{\mathbf{u}}_h^{k+\frac{1}{2}}, \mathbf{v}_h, q_h) + (\mathbf{f}, \mathbf{v}_h) \end{aligned} \quad (4.32)$$

for all  $(\mathbf{v}_h, q_h)$  in  $V_h \times Q_h$ . The strong consistency is easily seen by noting when evaluating (4.32) for an exact solution  $\mathbf{u}$  we have  $\mathbf{u}_h^k = \mathbf{u}_h^{k+1} = \mathbf{u}$ .

We defined the parameter  $W_K$  as:

$$W_K := \frac{\delta_K}{2\|\mathbf{u}\|_K} \min \left( 1, \frac{h\|\mathbf{u}\|_K \text{Re}}{2\|\mathbf{u}\|_{L^2}} \right)$$

where  $\delta_K$  is a small parameter. This definition was chosen based on empirical investigation. The proper selection of  $W_K$  for the existing methods is a nontrivial issue. We expect that the performance of this method can be properly tuned and improved through informed selection of this parameter and this is worth exploring in future work.

**Remark.** Like the related SUPG and GLS methods, this scheme also stabilizes the element spaces, allowing one to use non-LBB stable finite element pairs (such as  $\mathbb{P}^1/\mathbb{P}^1$ ) for velocity and pressure. This can be seen by observing that the expression for  $\mathcal{L}_{FIL}$  contains the term  $\sum_{K \in \mathcal{T}_h} h_K W_K (\nabla p_h, \nabla q_h)_{L^2(K)}$ , which adds a nonsingular negative discrete Laplacian matrix to the saddle-point system upon discretization, ensuring the nonsingularity of the system regardless of element choice [13].

**Theorem 4.3.** *At each iteration, the stabilized problem (4.32) is well-posed.*

**Proof.** Let

$$X := \left[ \sum_{K \in \mathcal{T}_h} \|(\bar{\mathbf{u}}_h \cdot \nabla) \mathbf{u}_h + \nabla p_h\|_K^2 \right]^{1/2}.$$

We utilize the following bound [24]:

$$\left| \sum_{K \in \mathcal{T}_h} h_K W_K (-\nu \Delta \mathbf{u}_h, (\bar{\mathbf{u}}_h \cdot \nabla) \mathbf{u}_h + \nabla p_h)_{L^2(K)} \right| \leq \frac{1}{2} \left( \nu \|\nabla \mathbf{u}_h\|_{L^2}^2 + X^2 \right) \quad (4.33)$$

We first show the coercivity of the bilinear form:

$$\begin{aligned} A((\mathbf{u}_h^{k+1}, p_h^{k+1}), (\mathbf{v}_h, q_h)) &= a(\mathbf{u}_h^{k+1}, \mathbf{v}_h) + c(\mathbf{u}_h^k, \mathbf{u}_h^{k+1}, \mathbf{v}_h) \\ &+ b(\mathbf{v}_h, p_h^{k+1}) - b(\mathbf{u}_h^{k+1}, q_h) + \mathcal{L}_{FIL}(\mathbf{u}_h^{k+1}, p_h^{k+1}; \bar{\mathbf{u}}_h^{k+\frac{1}{2}}, \mathbf{f}; \mathbf{v}_h, q_h) \end{aligned} \quad (4.34)$$

Set  $(\mathbf{v}_h, q_h) = (\mathbf{u}_h^{k+1}, p_h^{k+1})$ . Then:

$$\begin{aligned} A((\mathbf{u}_h^{k+1}, p_h^{k+1}), (\mathbf{u}_h^{k+1}, p_h^{k+1})) &= \nu \|\nabla \mathbf{u}_h\|_{L^2}^2 + c(\mathbf{u}_h^k, \mathbf{u}_h^{k+1}, \mathbf{u}_h^{k+1}) \\ &+ X^2 + \sum_{K \in \mathcal{T}_h} h_K W_K (-\nu \Delta \mathbf{u}_h^{k+1}, (\bar{\mathbf{u}}_h^{k+\frac{1}{2}} \cdot \nabla) \mathbf{u}_h^{k+1} + \nabla p_h^{k+1})_{L^2(K)} \end{aligned} \quad (4.35)$$

The second term on the right-hand side is zero by the skew-symmetry of  $c$ . Then by (4.33) we can group terms together and find:

$$\begin{aligned} A((\mathbf{u}_h^{k+1}, p_h^{k+1}), (\mathbf{u}_h^{k+1}, p_h^{k+1})) &> \frac{1}{2} (\nu \|\nabla \mathbf{u}_h^{k+1}\|_{L^2}^2 + X^2) \\ &\geq \frac{\nu}{2} \|\nabla \mathbf{u}_h^{k+1}\|_{L^2}^2 \\ &\geq C \|\mathbf{u}_h^{k+1}\|_V^2 \end{aligned} \quad (4.36)$$

The continuity of  $A$  and the right-hand side are obvious assuming that  $\mathbf{f}$ ,  $\bar{\mathbf{u}}_h^{k+\frac{1}{2}}$ , and  $\widehat{\bar{\mathbf{u}}}_h^{k+\frac{1}{2}}$  are bounded at each iteration  $k$ . The well-posedness follows. Note that a proof of well-posedness at each iteration does not imply the convergence of the iterative scheme to the desired solution; a rigorous proof of this (similar to that provided for the consistent scheme in the previous section) is still missing.

**Remark:** To obtain strong consistency when stabilizing along  $\bar{\mathbf{u}}$ , one may be tempted of setting

$$\begin{aligned} \mathcal{L}_h(\mathbf{u}_h, p_h; \bar{\mathbf{u}}_h, \mathbf{f} \mathbf{v}_h, q_h) &= \\ \sum_{K \in \mathcal{T}_h} h_K W_K (-\nu \Delta \mathbf{u}_h + (\mathbf{u}_h \cdot \nabla) \mathbf{u}_h + \nabla p_h - \mathbf{f}, (\bar{\mathbf{u}}_h \cdot \nabla) \mathbf{v}_h + \nabla q_h)_{L^2(K)} \end{aligned} \quad (4.37)$$

However, (4.37) turns out to be unstable. In fact, after testing against  $(\mathbf{u}^{k+1}, p^{k+1})$ , one obtains an

expression similar to (4.35), with the following term instead of  $X^2$ :

$$\sum_{K \in \mathcal{T}_h} h_K W_K ((\mathbf{u}_h^k \cdot \nabla) \mathbf{u}_h^{k+1} + \nabla p_h, (\bar{\mathbf{u}}_h^{k+\frac{1}{2}} \cdot \nabla) \mathbf{u}_h^{k+1} + \nabla p_h^{k+1})_{L^2(K)}$$

which is not guaranteed to be strictly positive in general due to the different convective fields on either side of the inner products.

## 5. Numerical Results and Discussion

In this section we test our methods on two 2D and two 3D test cases. Both 2D and 3D cases were tested on FreeFem++ using a 2017 MacBook Pro.

### 5.1. 2D Test Case 1: Flow Past a Step

In our first test, we solve the 2D Incompressible Navier-Stokes Equations at Reynolds numbers of 833 and 1000 in the domain pictured in Figure 3.

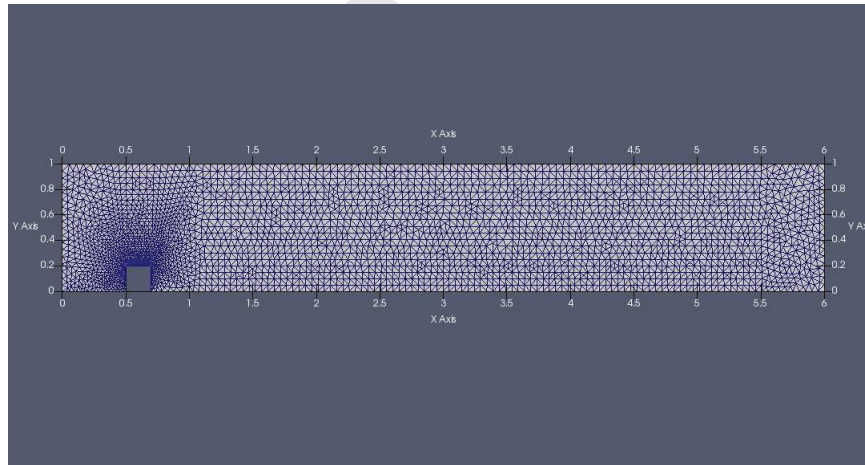


Fig. 3: Domain for the Flow Past a Step test case.

The domain is a  $6 \times 1$  rectangle with a  $.2 \times .2$  rectangular step along the bottom starting at  $x = .5$ . The flow becomes disturbed and a recirculation region develops past the step. We first computed a reference solution on a very fine mesh (38,280 DOF) using standard Picard iterations to a high level of accuracy (stopping tolerance of  $10^{-8}$  in the relative  $L^2$  velocity norm between consecutive iterates).



Next, we computed stabilized solutions on different mesh levels using the different techniques discussed, including both the streamline-diffusion type and strongly consistent methods.

For the purposes of comparison, we also computed solutions stabilized with the classical streamline diffusion and SUPG methods. For all computations, we used a Picard-type approach and iterated until the difference in velocity  $L^2$  norm between iterations was below  $1e-3$ . For all tests we used  $P^2/P^1$  finite elements for velocity and pressure respectively, and set  $\mu = .2$ ,  $\delta_K = .1$ . We report the results in Table 1.

Note that as the reference solution is a numerical one computed on a much finer mesh than our stabilized solutions, *we only expect convergence up to the level of interpolation error*.

Flow Past a Step: Weakly Consistent Deconvolution Stabilization vs Streamline Diffusion						
Re	Ref. Iter.	DOF	Deconv. It.	$\ u_D - u\ _{L^2} / \ p_D - p\ _{L^2}$	SD Iter.	$\ u_S - u\ _{L^2} / \ p_S - p\ _{L^2}$
833	52	17292	23	.0029/.0133	30	.0035/.0143
833	52	28623	28	.0028/.0106	43	.0013/.0059
1000	89	18192	28	.0046/.0186	40	.0051/.0139
1000	89	28623	34	.0039/.0143	56	.0028/.0056
Flow Past a Step: Strongly Consistent Deconvolution Stabilization vs SUPG						
Re	Ref. Iter.	DOF	Deconv. It.	$\ u_D - u\ _{L^2} / \ p_D - p\ _{L^2}$	SUPG It.	$\ u_S - u\ _{L^2} / \ p_S - p\ _{L^2}$
833	52	17292	29	.0034/.0141	60	.0035/.0148
833	52	28623	39	.0016/.0058	52	.0013/.0048
1000	89	17292	39	.0051/.0143	DNC	NA/NA
1000	89	28623	55	.0028/.0056	85	.0019/.0059

Table 1: Numerical results, 2D flow past a step. Ref. Iter. indicates to the number of iterations required by the reference solution.

Our methods outperform the standard methods in all tests, requiring significantly fewer iterations to reach convergence in each instance. While the weakly consistent methods are known to suffer from reduced accuracy, this did not seem to have significant impact on this case except for  $Re=1000$  on the fine mesh, where weakly consistent deconvolution stabilization was less accurate than other methods.

Referring to Figure 4, we plot a comparison of the convergence of deconvolution stabilization vs SUPG for  $Re=1000$  for both the coarse (17,292 DOF, top) and moderate (28,623 DOF, bottom) meshes. Note that standard Picard failed to converge at these mesh levels. On the coarse mesh, we see that our method (blue) converges monotonically up to interpolation error in both velocity and pressure while for SUPG (red) the convergence becomes oscillatory, particularly for the pressure, failing to converge. While SUPG converges on the fine mesh, its convergence is significantly slower than deconvolution. Fig. 5 shows a the velocity streamlines for the case  $Re=1000$  colored according to the magnitude of  $u_h$  and  $\bar{u}_h$ , again

demonstrating the filter's ability to identify and stabilize low-convection regions.

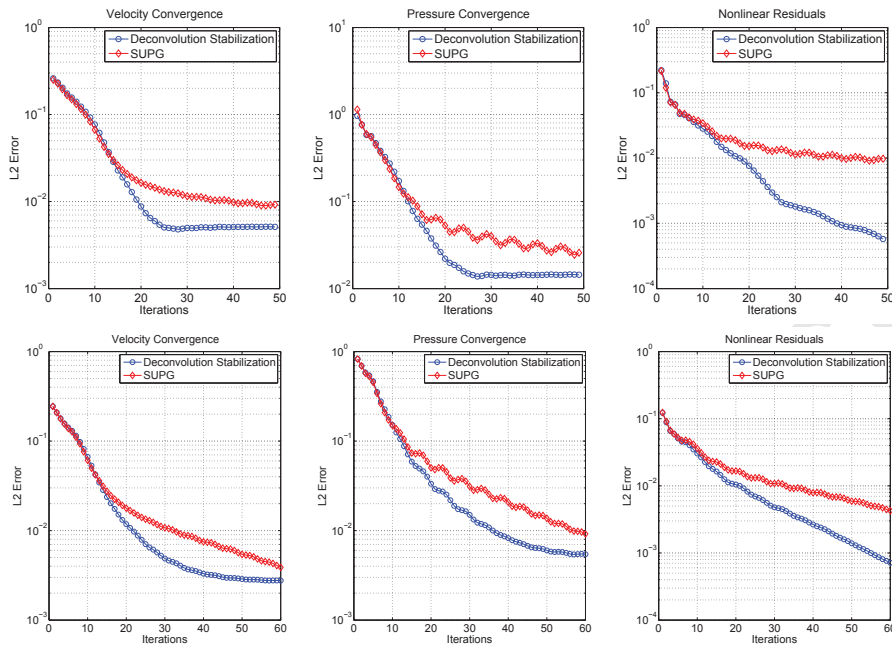


Fig. 4: Convergence, Test Case 1.  $Re=1000$ . Top: 17292 DOF (coarse); Bottom: 28623 DOF (Fine).

## 5.2. 2D Test Case 2: Flow in a Curved Pipe

We follow an identical procedure as before for our next 2D case, the curved pipe shown previously in Figs. 1 and 2. We compare our stabilized solutions for different mesh levels to a standard solution computed on a fine mesh (47,070 DOF) for Reynolds numbers 600 and 667 and report the results in Table 2. Although the two Reynolds numbers appear close together, the behavior of the flow is quite different. For even slightly higher Reynolds numbers, such as 700, the solution is no longer steady, even on extremely fine meshes. This test is designed to showcase our stabilization method at the upper limit of the steady flow regime. Our approach results in significantly fewer iterations to reach convergence while maintaining the same order of accuracy when compared to traditional stabilization techniques. For this test case, we do observe that the weakly consistent methods appear slightly less accurate when compared to the strongly consistent methods, particularly on the fine meshes.

The sharp increase in the required number of iterations (for all methods) for what appears to be a small increase in Reynolds number is expected based on the critical nature of this flow regime.

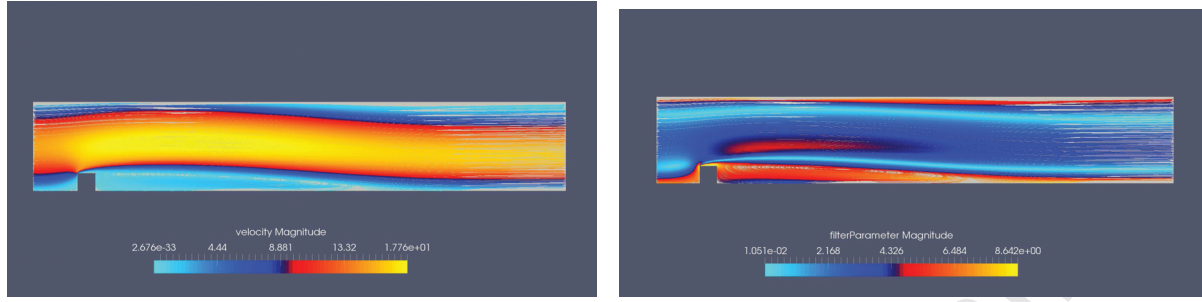


Fig. 5: Results for 2D flow past a step, Re=1000. Left: Velocity streamlines colored according to velocity magnitude; Right: Regions requiring stabilization as identified by the filter.

Curved Pipe: Weakly Consistent Deconvolution Stabilization vs Streamline Diffusion						
Re	Ref. Iter.	DOF	Deconv. It.	$\ u_D - u\ _{L^2} / \ p_D - p\ _{L^2}$	SD Iter.	$\ u_S - u\ _{L^2} / \ p_S - p\ _{L^2}$
600	53	11879	21	.0192/.0448	44	.0222/.0458
600	53	23015	35	.0076/.0191	42	.00502/.0103
667	96	11879	30	.0308/.0934	54	.0251/.0571
667	96	23015	38	.0089/.0231	62	.0066/.0108
Curved Pipe: Strongly Consistent Deconvolution Stabilization vs SUPG						
Re	Ref. Iter.	DOF	Deconv. It.	$\ u_D - u\ _{L^2} / \ p_D - p\ _{L^2}$	SUPG It.	$\ u_S - u\ _{L^2} / \ p_S - p\ _{L^2}$
600	53	11879	36	.0166/.0440	49	.0163/.0435
600	53	23015	39	.0035/.0075	53	.0025/.00592
667	96	11879	61	.0187/.0453	85	.0215/.0580
667	96	23015	61	.0053/.0101	95	.0035/.0078

Table 2: Numerical results, 2D curved pipe.

**Remark:** As mentioned before, our scheme also stabilizes the pressure and element spaces, enabling us to use non-LBB inf-sup compatible pairs for velocity and pressure (such as  $\mathbb{P}^1/\mathbb{P}^1$ ). We compute the same 2D curved pipe test at Re=667 using  $\mathbb{P}^1/\mathbb{P}^1$  on the same mesh level as our fine solution and report the results in Table 3.

Curved Pipe: Deconvolution Stabilization vs SUPG; Stabilized $\mathbb{P}^1/\mathbb{P}^1$						
Re	Ref. Iter.	DOF	Deconv. It.	$\ u_D - u\ _{L^2} / \ p_D - p\ _{L^2}$	SUPG It.	$\ u_S - u\ _{L^2} / \ p_S - p\ _{L^2}$
667	96	16032	59	.0170/.0469	71	.0163/.0432

Table 3: Numerical results, 2D curved pipe with stabilized  $\mathbb{P}^1/\mathbb{P}^1$  elements.

This element space greatly reduces the degrees of freedom (16,032 rather than 47,070). The time per iteration for one (non-stabilized,  $\mathbb{P}^2/\mathbb{P}^1$ ) fine mesh solution was 2.64 seconds; for stabilized  $\mathbb{P}^1/\mathbb{P}^1$  we observed 1.83 seconds per iteration. As expected, we lose accuracy with this element space, however. We again see faster convergence and similar error behavior using our method as compared to SUPG.

### 5.3. 3D Test Case 1: Curved Pipe

Our next test case is a three-dimensional version of the curved pipe designed to demonstrate our method's applicability to 3D problems. We solve the 3D INS equations at  $Re=700$  in the domain pictured in Figure 6. For this test, we computed a solution without stabilization using standard Picard iterations on a fine mesh (155,872 DOF). We then computed a stabilized solutions on a coarse mesh (61,391 DOF) using our strongly consistent method and SUPG stabilization. We validated our solutions by comparing the value of the pressure along the center plane of the pipe as pictured in Figure 6.

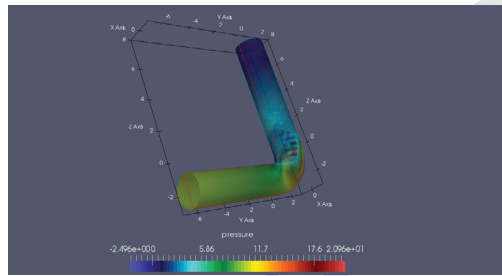


Fig. 6: We compare the pressure along the pictured curve (red).

We used the same tolerance and values for  $\delta$  and  $\mu$  as before. We again observed improved performance; standard Picard required 34 iterations to converge on the fine mesh and did not converge on the coarse mesh. The coarse solution stabilized with SUPG converged in 47 iterations, while the solution stabilized with our techniques converged in 32 iterations. In Figure 6, we display the centerline of the vessel, where we compare the pressure solutions. We observe that the stabilized solutions show good agreement with the fine mesh solution, with no significant difference between the Deconvolution and SUPG solutions (Fig. 7).

### 5.4. 3D Test Case 2: FDA Nozzle Benchmark, $Re=500$

For our final test case we consider the FDA Nozzle Benchmark case [1] for  $Re=500$ . We use an identical geometrical configuration as found in [21]. The geometry is shown in Figure 8. This test case differs from our previous test cases in that the primary instabilities arise from the high-convection; we seek to show that our stabilization method remains a viable choice in such instances. We note that our filtering method in no way excludes unstable high-convection regions, but merely aims to capture other, additional types

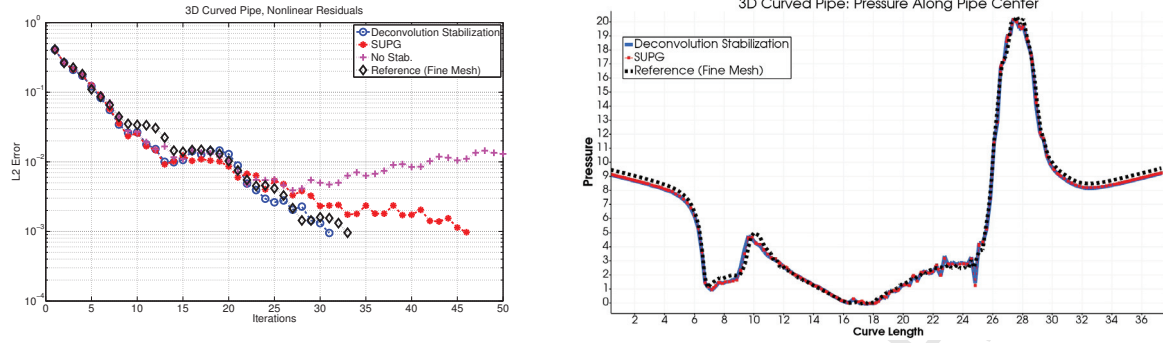


Fig. 7: Results for 3D curved pipe test. Left: convergence residuals. Note the solution does not converge on the coarse mesh without stabilization; Right: Pressure along the curve pictured in in Figure 6.

of instability as well. Therefore, we do not necessarily expect our methods to outperform standard techniques; however we seek to verify that they remain competitive.

We set the density  $\rho = 1.056 \text{ g/cm}^3$  and viscosity  $\nu = .035 \text{ g/cm}\cdot\text{s}$  and prescribe a Poiseuille parabolic inflow profile with a flow rate of 5.2062 ml/s. We again set  $\mu = .2$ ,  $\delta_K = .1$ . We monitor convergence by comparing the difference in velocity  $L^2$  norm between consecutive iterations, and stop iterations when this falls below 1e-3. We will also monitor the pressure drop  $p(0,0,-4) - p(0,0,0)$  between iterations to cross-validate the velocity convergence criterion.

We run our simulations with  $\mathbb{P}^2/\mathbb{P}^1$  finite elements on a coarse mesh containing 52,895 tetrahedra (243,958 total DOF), an order of magnitude coarser than the meshes used in [21]. At this mesh level, a Picard iteration using standard Galerkin techniques fails to converge, necessitating the use of stabilization techniques. We compare our strongly consistent deconvolution scheme with SUPG in terms of both convergence and agreement with the measured solution. The convergence results are shown in Figure 9.

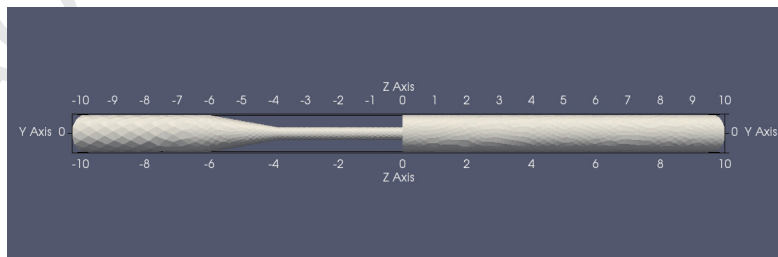


Fig. 8: Geometry for FDA test case.

SUPG converges slightly faster than the deconvolution scheme (19 iterations compared to 24) in terms

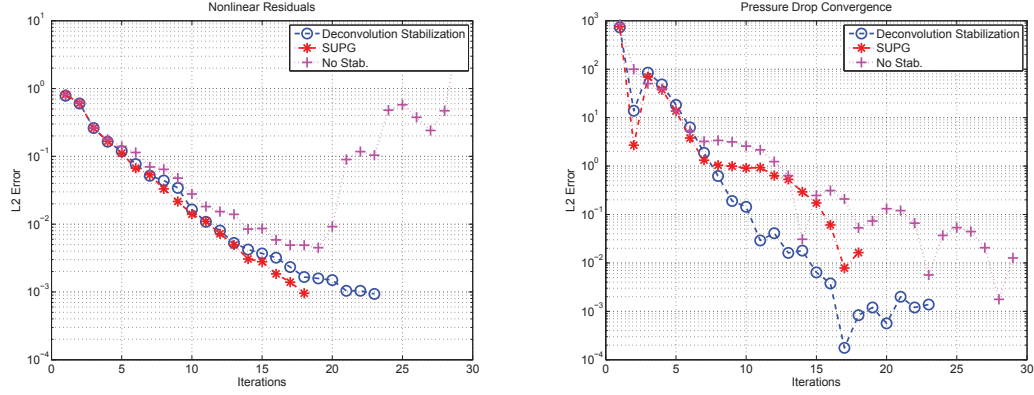


Fig. 9: Left: FDA nonlinear residuals; Right: FDA pressure drop residuals

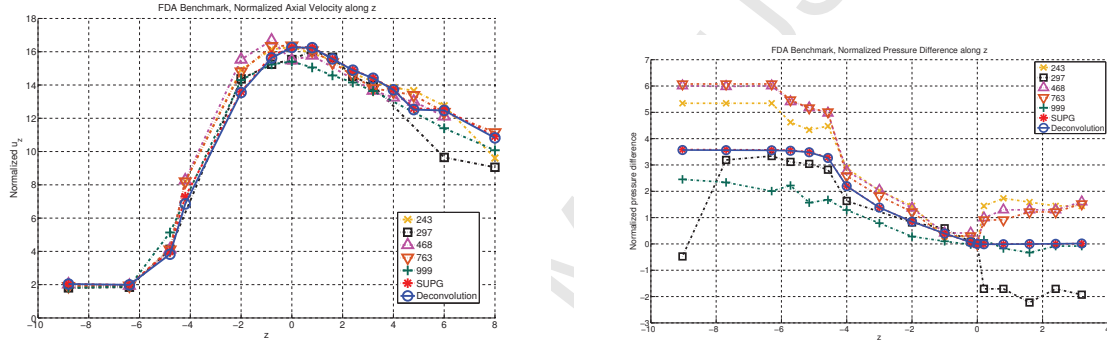


Fig. 10: Comparison with experimental data, FDA test case. Left: centerline velocity, right: pressure drop.

of our velocity residual, however we note that the pressure drop converges more steadily and rapidly for deconvolution filtering. We see that the iterations fail to converge without stabilization.

Comparing our results to the benchmark data (labeled in accordance with [1]), we find our normalized velocity and pressure drop along the centerline in strong agreement with the reference experimental data (Fig. 10). We do not observe any noteworthy difference between SUPG and deconvolution filtering in terms of accuracy.

Qualitatively, we see that in this case the nonlinear filter does indeed identify high-convection regions as requiring stabilization, in addition to the recirculation regions (Fig. 11). While this method was not designed specifically for stabilizing high-convection regions, it still can be used for this purpose. In particular, this suggests that our method remains a good choice for problems in which one encounters both convective and non-convective instabilities.

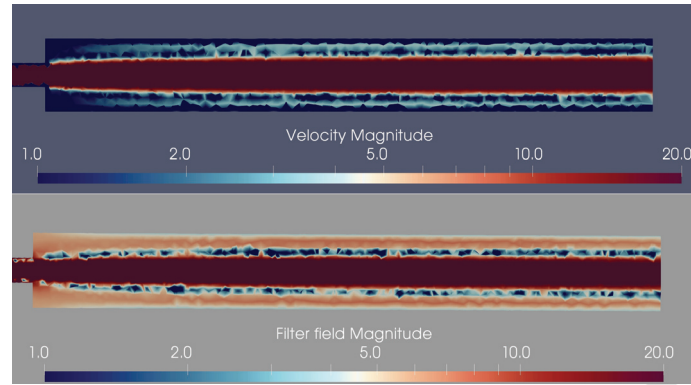


Fig. 11: Top: velocity field  $u$ . Bottom: filtered velocity field  $\bar{u}$ .

## 6. Conclusions

In this paper we present a method for the stabilization of the incompressible NS equations in both steady and unsteady regimes. We focused specifically on the steady case. Our method specifically considers the case when small-scale dynamics are activated by geometrical features of the domain of interest rather than high convective fields. This is the case in many computational hemodynamic applications, when in fact small local features of the vascular district may trigger some local dynamics that challenge the numerical approximation - in particular for the meshing. We borrow from Large Eddy Simulation turbulence modeling to identify a region where the flow is not smooth and requires stabilization. This is done by exploiting the deconvolution filter function formerly advocated by W. Layton and collaborators. Using this tool for detecting regions requiring additional numerical diffusivity, we extended classical streamline diffusion and strongly consistent methods traditionally based on the strength of the convective term. We briefly analyzed the methods stemming from this idea, showing that in cases of flow disturbances triggered by the geometry, the present approach is more effective in dumping numerical instabilities. Next steps will be on the one hand the theoretical analysis of the convergence rate, in particular for SUPG-like methods, where we expect that the convergence rate in an appropriate norm depends on the polynomial degree. We also plan to use the methods in extensive numerical simulation campaigns in cardiovascular problems (the so-called Computer Aided Clinical Trials).

- [1] Computational Fluid Dynamics Round Robin Study, <https://fdacfd.nci.nih.gov/>.
- [2] Y Bazilevs, VM Calo, JA Cottrell, TJR Hughes, A Reali, and G Scovazzi. Variational multiscale residual-based turbulence modeling for large eddy simulation of incompressible flows. *Computer Methods in Applied Mechanics and Engineering*, 197(1-4):173–201, 2007.
- [3] L Bertagna, A Quaini, and A Veneziani. Deconvolution-based nonlinear filtering for incompressible flows at moderately large reynolds numbers. *International Journal for Numerical Methods in Fluids*, 14(8):463–488, 2016.



- [4] J Borggaard, T Iliescu, and JP Roop. A bounded artificial viscosity large eddy simulation model. *SIAM J. Numer. Anal.*, 47:622–645, 2009.
- [5] AL Bowers and LG Rebholz. Numerical study of a regularization model for incompressible flow with deconvolution-based adaptive nonlinear filtering. *Comput. Methods Appl. Mech. Eng.*, 258:1–12, 2013.
- [6] Haim Brezis. *Opérateurs maximaux monotones et semi-groupes de contractions dans les espaces de Hilbert*, volume 5. Elsevier, 1973.
- [7] Haim Brezis. *Functional analysis, Sobolev spaces and partial differential equations*. Springer Science & Business Media, 2010.
- [8] Alexander N Brooks and Thomas JR Hughes. Streamline upwind/Petrov-Galerkin formulations for convection dominated flows with particular emphasis on the incompressible Navier-Stokes equations. *Computer methods in applied mechanics and engineering*, 32(1-3):199–259, 1982.
- [9] V.J. Ervin, W.J. Layton, and J.M.L. Maubach. Adaptive defect-correction methods for viscous incompressible flow problems. *SIAM J. Numer. Anal.*, 37(4):1165–1185, 2000.
- [10] Leopoldo P Franca and Thomas JR Hughes. Convergence analyses of Galerkin least-squares methods for symmetric advective-diffusive forms of the Stokes and incompressible Navier-Stokes equations. *Computer Methods in Applied Mechanics and Engineering*, 105(2):285–298, 1993.
- [11] Vivette Girault and Pierre-Arnaud Raviart. *Finite element methods for Navier-Stokes equations: theory and algorithms*, volume 5. Springer Science & Business Media, 2012.
- [12] T. J R Hughes and A. Brooks. Multi-dimensional upwind scheme with no crosswind diffusion. *American Society of Mechanical Engineers, Applied Mechanics Division, AMD*, 34, 1979.
- [13] Thomas JR Hughes, Leopoldo P Franca, and Marc Balestra. A new finite element formulation for Computational Fluid Dynamics: Circumventing the Babuška-Brezzi condition: A stable Petrov-Galerkin formulation of the Stokes problem accommodating equal-order interpolations. *Computer Methods in Applied Mechanics and Engineering*, 59(1):85–99, 1986.
- [14] Ohannes A Karakashian. On a Galerkin-Lagrange multiplier method for the stationary Navier-Stokes equations. *SIAM Journal on Numerical Analysis*, 19(5):909–923, 1982.
- [15] S. Kaya, W.J. Layton, and B. Riviere. Subgrid stabilized defect correction methods for the Navier-Stokes equations. *SIAM J. Numer. Anal.*, 44(4):1639–1654, 2006.
- [16] W. Layton, H.K. Lee, and J. Peterson. A defect-correction method for the incompressible Navier-Stokes equations. *Applied Mathematics and Computation*, 129:1–19, 2002.
- [17] W Layton, LG Rebholz, and C Trenchea. Modular nonlinear filter stabilization of methods for higher reynolds numbers flow. *J. Math. Fluid Mech.*, 14:325–354, 2012.
- [18] William J Layton and Leo G Rebholz. *Approximate deconvolution models of turbulence: analysis, phenomenology and numerical analysis*, volume 2042. Springer Science & Business Media, 2012.
- [19] W.J. Layton. A connection between subgrid scale eddy viscosity and mixed methods. *Math. Comput.*, 133:147–157, 2002.
- [20] J Leray. Essai sur le mouvement d’un fluide visqueux emplissant l’espace. *Acta. Math.*, 63:193–248, 1934.
- [21] T. Passerini, Quaini A., U. Villa, A. Veneziani, and S. Canic. Validation of an open source framework for the simulation of blood



- flow in rigid and deformable vessels. *International Journal for Numerical Methods in Biomedical Engineering*, 29(11):1192–1213, 2013.
- [22] Alfio Quarteroni. *Numerical models for differential problems*. Springer Science & Business Media, 2010.
- [23] Alfio Quarteroni and Alberto Valli. *Numerical approximation of partial differential equations*, volume 23. Springer Science & Business Media, 2008.
- [24] Hans-Gorg Roos, Martin Stynes, and Lutz Tobiska. *Robust Numerical Methods for Singularly Perturbed Differential Equations, Second Edition*. Springer, 2008.
- [25] S Salsa. *Partial differential equations in action, from modeling to theory*. Springer, 2009.
- [26] R. Temam. *Navier-Stokes equations*. Elsevier, North-Holland, 1991.
- [27] Stefan Turek. *Efficient Solvers for Incompressible Flow Problems: An Algorithmic and Computational Approach*, volume 6. Springer Science & Business Media, 1999.